Role of Renner Teller and Spin−Orbit Interaction in the Dynamics of the $O(^3P) + CH_2ICl$ Reaction

X. Gao, J. Essex-Lopresti, S. Munro, M. P. Hall, D. J. Smith, and R. Grice*

Chemistry Department, University of Manchester, Manchester, M13 9PL, U.K.

Received: September 22, 1997; In Final Form: November 24, 1997

Reactive scattering of $O(^3P)$ atoms with CH_2ICl molecules has been measured at initial translational energies $E \sim 46$ and 17 kJ mol^{-1} using a supersonic beam of O atoms seeded in He and Ne buffer gases generated from a high-pressure microwave discharge source. At the higher initial translational energy, the IO product scattering can be resolved into two components; one showing forward and backward peaking with a product translational energy distribution peaking at low energy with a tail extending out to higher energy, and the other that peaks in the backward direction with higher product translational energy. At lower initial translational energy, the IO product scattering does not allow the resolution of two components but peaks in the backward direction with a higher product translational energy than for scattering in the forward hemisphere. The slow component is attributed to dissociation of a long-lived $OICH_2Cl$ complex formed by intersystem crossing from the initial triplet $^3A''$ potential energy surface to the underlying singlet $^1A'$ potential energy surface. The fast component is attributed to direct reaction over the triplet potential energy surface with the sharp backward peaking arising from reaction on the $^3\Pi_2$ and $^3\Pi_1$ spin multiplet surfaces in near collinear $OICH_2Cl$ configurations and the scattering in the sideways and forward directions arising from reaction on the $^3A''$ Renner Teller surface in strongly bent configurations. The contribution of the slow component is approximately one-third that of the fast component to the total reaction cross section for IO product scattering.

Introduction

Recent crossed molecular beam studies[1−5] of the reactive scattering of ground-state $O(^3P)$ atoms with alkyl and allyl iodide molecules have shown the importance of intersystem crossing from the initial triplet potential energy surfaces to the underlying singlet potential energy surface. Direct dynamics over the triplet potential energy surface result in IO product formed with high translational energy, whereas the singlet potential energy surface supports a long-lived OIR intermediate complex that yields IO product with low translational energy and in some cases[1,2,6,7] HOI product formed via a five-membered ring transition state. In the case of alkyl and allyl iodides,[1−3] the direct scattering appears as enhanced backward scattering of IO product, whereas enhanced sideways scattering is observed[4] for CF_3I and little[5] direct scattering is observed for CF_3CH_2I. This variation in the direction and extent of direct IO scattering has been related[4] to the effect of charge transfer interaction of the form OI^+R^- on the Renner Teller splitting of the triplet potential energy surface in strongly bent configurations. To test the validity of this hypothesis, studies have been undertaken on further substituted iodomethane molecules varying the electron affinity of the departing radical R. Results are reported here on the reaction of chloroiodomethane molecules that may also be of some significance in the iodine chemistry of the upper atmosphere[8]:

$$O(^3P) + CH_2ICl \rightarrow IO(^2\Pi_{3/2}) + CH_2Cl \qquad (1)$$

Experimental Section

The cross-beam scattering machine was the same as that used[5] to study the reaction of $O(^3P)$ atoms with CF_3CH_2I molecules with improved cryopumping of the cross beam source differential pumping. The O atom beam was produced from a high-pressure microwave discharge source[9] using an ∼8% mixture of O_2 in excess He or Ne buffer gas. The O atom beam velocity distribution was measured by a beam monitor quadrupole mass spectrometer using pseudorandom cross correlation time-of-flight analysis[10] to gain the velocity parameters quoted in Table 1. The cross beam issued from a glass nozzle diameter of ∼0.2 mm with a stagnation pressure of ∼60 mbar maintained by a reservoir at a temperature of ∼25 °C. The beam velocity distribution was measured by the rotatable mass spectrometer detector to gain the velocity parameters quoted in Table 1.

TABLE 1: Beam Velocity Distributions: Peak Velocity v_{pk}, Full Width at Half Maximum Intensity v_{wd}, and Mach Number M

beam	v_{pk}, m s^{-1}	v_{wd}, m s^{-1}	M
O(He)	2450	740	6
O(Ne)	1440	430	6
CH_2ICl	470	195	4

Results

Angular distribution measurements of IO number density give signal rates of ∼80 and 50 counts s^{-1} against backgrounds of ∼20 and ∼30 counts s^{-1} for O atoms seeded in He and Ne buffer gases. The laboratory angular distributions of IO scattering shown in Figures 1 and 2 both peak close to the centroid vector but with a shoulder to wider angles in Figure 1 for O atoms seeded in He buffer gas. The laboratory velocity distributions of IO product scattering shown in Figures 3 and 4 were measured with integration times of ∼3000−5000 s to yield signal-to-noise ratios of ∼10−30 at the peaks of the distributions. Kinematic analysis of these data employed the forward convolution method[11] with a differential cross section expressed as a product of an angular function $T(\theta)$ and a velocity function

S1089-5639(97)03079-X CCC: $15.00
Published on Web 02/20/1998

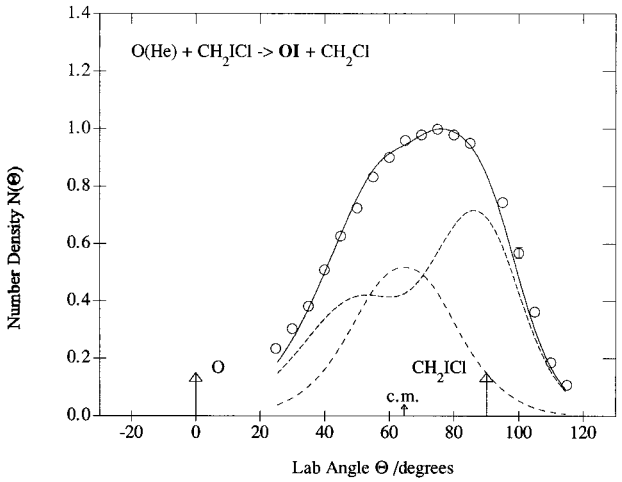

Figure 1. Laboratory angular distribution (number density) of IO reactive scattering from O + CH_2ICl at initial translational energy E of ~46 kJ mol^{-1}. Solid line shows fit of the kinematic analysis; broken curves show contributions of fast and slow components.

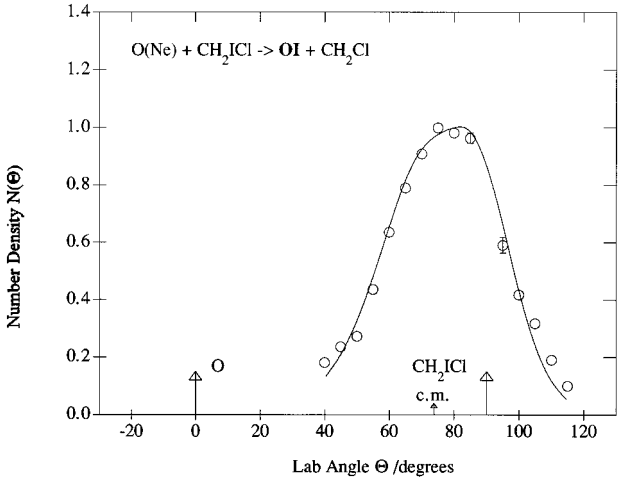

Figure 2. Laboratory angular distribution (number density) of IO reactive scattering from O + CH_2ICl at initial translational energy E of ~17 kJ mol^{-1}.

$U(u,\theta)$, which may depend parametrically on center-of-mass scattering angle θ:

$$I_{cm}(\theta,u) = I(\theta)U(u,\theta) \qquad (2)$$

The IO product scattering for O atoms seeded in He buffer gas is expressed as a sum of two components as shown in Figure 5. The slow component shows forward and backward peaking with a product translational energy distribution peaked at low energy with a tail extending out to higher energy. The fast component shows sharp backward peaking with scattering extending into the forward hemisphere and a product translational energy distribution peaked at high energy. In each case, the product translational energy distribution is independent of scattering angle. However two components could not be separately resolved for O atoms seeded in Ne buffer gas but the IO product angular distribution in Figure 6 also favors the backward direction with a product translational energy distribution which shifts to lower energy as the scattering moves round into the forward hemisphere. The peak E'_{pk} and average E'_{av} product translational energies are listed in Table 2 together with the initial translational energies E and the reaction exoergicity ΔD_0 estimated from the IO bond energies of Radlein et al.[12] and Buss et al.[13] and the thermochemical kinetics measurements of Seetula,[14] Holmes and Lossing,[15] and Bedjanian et al.[16] The relative contribution of the fast and slow components of Figure 5 to the total reaction cross section was obtained by integration over the differential cross sections:

$$Q \propto \int_0^{\pi} T(\theta) \sin\theta \, d\theta \int_0^{u_{max}} U(u) \, du \qquad (3)$$

This yields a ratio Q(slow)/Q(fast) of ~0.35 ± 0.05. The sharp backward peaking contributes only a small fraction of the total reaction cross section despite its prominence in the laboratory angular distribution of IO scattering.

Discussion

Figure 7 shows the reaction profile for the triplet $^3A''$ potential energy surface for O(^{3}P) + CH_2ICl that is intersected in the entrance valley in bent OIC configurations by the singlet $^1A'$ potential energy surface that supports a bound $OICH_2Cl$ intermediate. The ab initio calculations of Marshall[17] and Morokuma[18] support this picture and predict, a bent geometry with an interbond angle β of 108° and a well depth E_0 of ~155 kJ mol^{-1} with respect to reaction products for the singlet $OICH_3$ intermediate. This well depth has also been adopted for the $OICH_2Cl$ intermediate in Figure 7. Indeed a bound $OICH_2Cl$ intermediate has been observed in a near-infrared photolysis study[19] of an O_3:CH_2ICl complex in an Ar matrix and this may be identified with the singlet intermediate of Figure 7. The slow component of IO scattering in Figure 5 with almost equal forward and backward peaking and a product translational energy distribution peaked at low energy may be identified with reaction via a long-lived singlet $OICH_2Cl$ complex. However, the fast component of IO scattering in Figure 5 peaks sharply in the backward direction with lower intensity extending into the forward hemisphere and a product translational energy distribution peaked at higher energy and may be identified with direct reaction over the triplet potential energy surface. The IO scattering at lower initial translational energy E of ~17 kJ mol^{-1} cannot be resolved into two such components, but the strongly backward peaked angular distribution in Figure 6 with increased product translational energy in the backward direction again suggests that a two-component mechanism applies in this case also.

The IO product scattering from the O + CF_3I reaction has also been resolved into two components recently[4] with a slow component attributed to reaction via a long-lived singlet $OICF_3$ complex, which gives angular and product translational energy distributions similar to the slow component of O + CH_2ICl. However, the fast component for O + CF_3I shows sideways scattering with only a weak tendency toward backward scattering. On the other hand, the angular distributions for O(^{3}P) atoms reacting with C_2H_5I, $(CH_3)_2CHI$, $(CH_3)_3CI$ and C_3H_5I molecules[1-3] all show enhanced IO product scattering in the backward direction with increased product translational energy that is similar to the IO scattering for O + CH_2ICl in Figure 6. The sideways scattering for O + CF_3I has been attributed[4] to direct dynamics over the triplet $^3A''$ potential energy surface in strongly bent configurations with the O atom approaching the CF_3I molecule in the broadside orientation. Correspondingly, the strongly backward peaked scattering observed for O + CH_2ICl must correspond to the O atom approaching the I atom of the CH_2ICl molecule in a direction nearly collinear with the CI bond.

Figure 8 illustrates the Renner Teller splitting[20] of the triplet $^3\Pi$ potential energy surface as a function of the OIC interbond angle β where $\beta = 180°$ denotes the collinear configuration. In

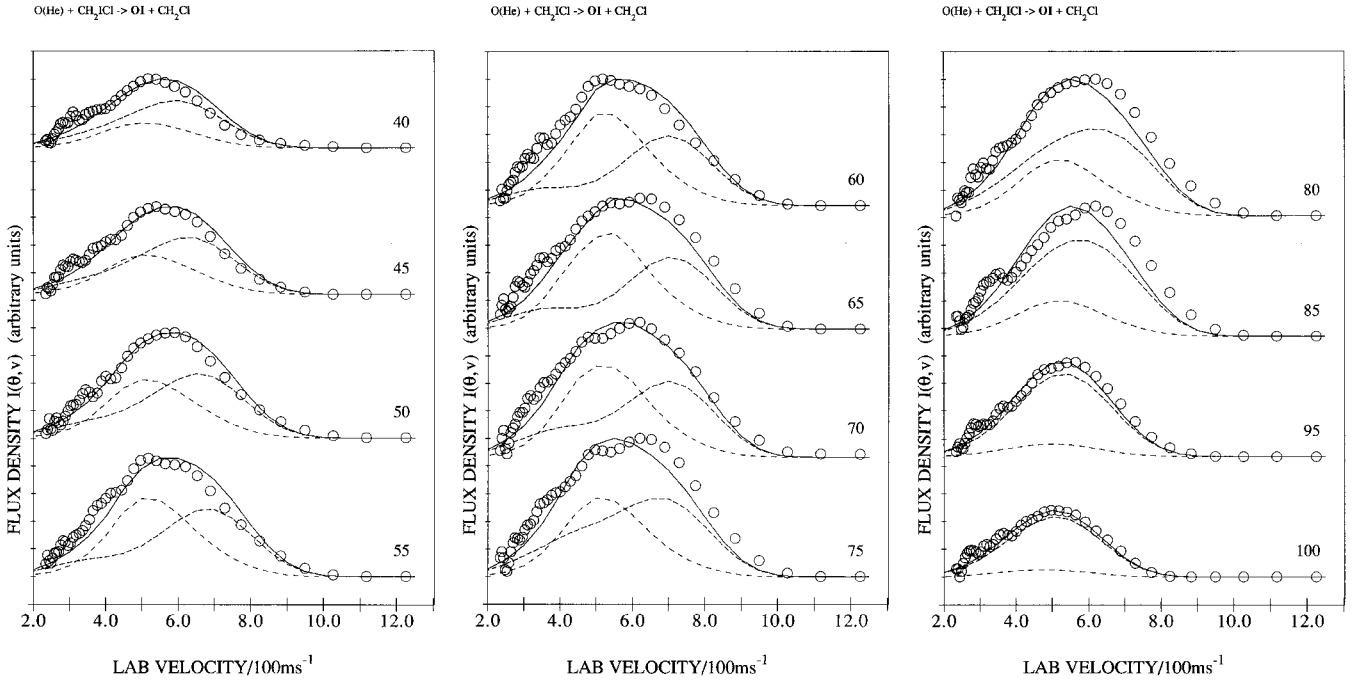

Figure 3. Laboratory velocity distributions (flux density) of reactively scattered IO from O + CH_2ICl at an initial translational energy E of ~46 kJ mol^{-1}. Solid line shows fit of the kinematic analysis; broken curves show contributions of fast and slow components. Relative uncertainies are ~0.1 at the peak, increasing to ~1 at the highest and lowest velocities of the distributions.

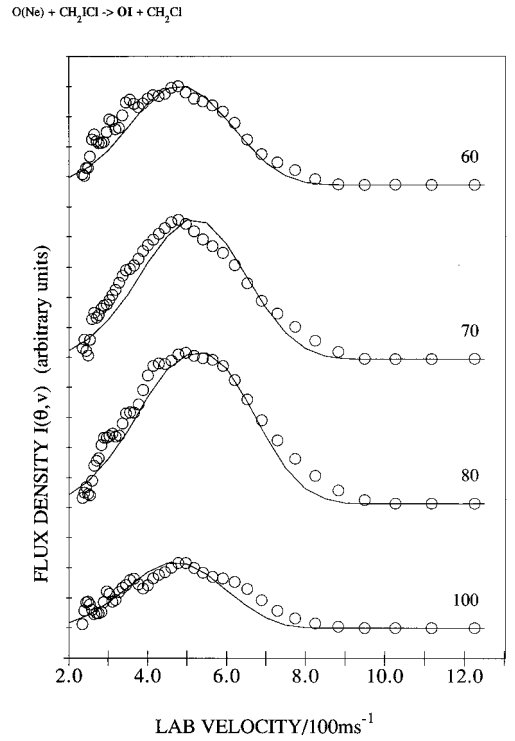

Figure 4. Laboratory velocity distributions (flux density) of reactively scattered IO from O + CH_2ICl at an initial translational energy E of ~17 kJ mol^{-1}.

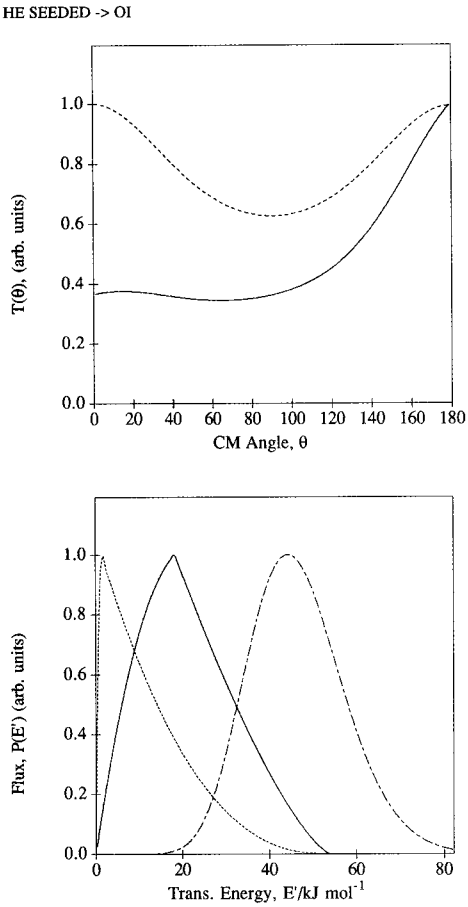

Figure 5. Angular functions $T(\theta)$ and translational energy distributions P(E′) for IO products from O + CH_2ICl at initial translational energy E of ~46 kJ mol^{-1}. Solid line denotes the fast component, broken line the slow component. Dot−dashed line denotes the distribution of initial translational energy.

the absence of spin−orbit interaction, the $^3\Pi$ potential energy surface splits into an upper $^3A'$ surface, which favors the collinear configuration and a lower $^3A''$ surface which favors bent configurations. However spin−orbit interaction splits the $^3\Pi$ surface into spin multiplet components $^3\Pi_2$, $^3\Pi_1$, $^3\Pi_{0^+}$, $^3\Pi_{0^-}$ in the collinear configuration and in bent configurations the symmetries of the spin multiplet components are denoted by a′ and a″. In the collinear configuration, the splitting of the triplet potential energy surface is determined by spin−orbit interaction but when the interbond angle β decreases to the crossing angle β_c where the effects of spin−orbit and Renner Teller interactions

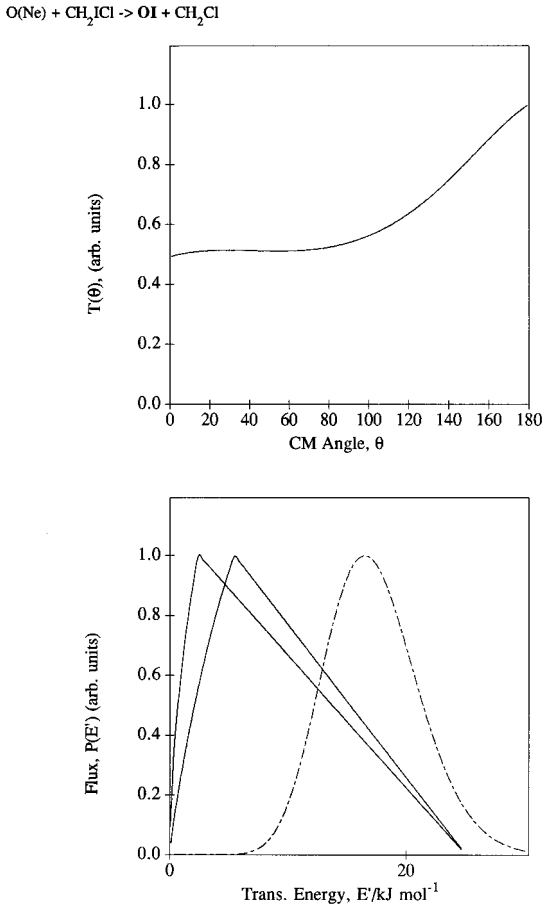

Figure 6. Angular function $T(\theta)$ and translational energy distributions P(E′) for IO products from O + CH_2ICl at initial translational energy E of ∼17 kJ mol^{-1}. Left-hand product translational energy distribution for forward scattering, right-hand backward scattering.

TABLE 2: Reaction Energetics (kJ mol^{-1}): Initial Translational Energy E, peak product Translational Energy E'_{pk}, Average Product Translational Energy E'_{av}, and Reaction Exoergicity ΔD_0

E	E'_{pk}		E'_{av}		ΔD_0
	fast	slow	fast	slow	8 ± 10
46	18	2	21	12	
	backward	forward	backward	forward	
17	6	3	10	9	

become comparable, then avoided crossings occur between spin multiplet components of the same symmetry as shown in Figure 8. For further decrease in the interbond angle β, the triplet potential energy surfaces become characterized as ^{3}A′ and ^{3}A″ Renner Teller surfaces with subsidiary splitting into a′ and a″ spin multiplet components.[1]

Both the $^3\Pi_2$ and $^3\Pi_1$ spin multiplet components in the collinear configuration and the ^{3}A″ Renner Teller surface in more strongly bent configurations correlate with ground state IO($^2\Pi_{3/2}$) + CH_2Cl reaction products as shown in Figure 7. Hence, in the absence of an intervening potential energy barrier, strongly backward peaked scattering will arise from reaction over the $^3\Pi_2$ and $^3\Pi_1$ potential energy surfaces in the near collinear configuration and sideways scattering will arise from direct dynamics over the ^{3}A″ potential energy surface in configurations more strongly bent than the crossing angle β_c. Consequently, the balance of backward peaking and sideways scattering depends on the relative strength of the spin−orbit and Renner Teller interactions, which determines the value of the crossing angle β_c. It has been argued previously[4] that

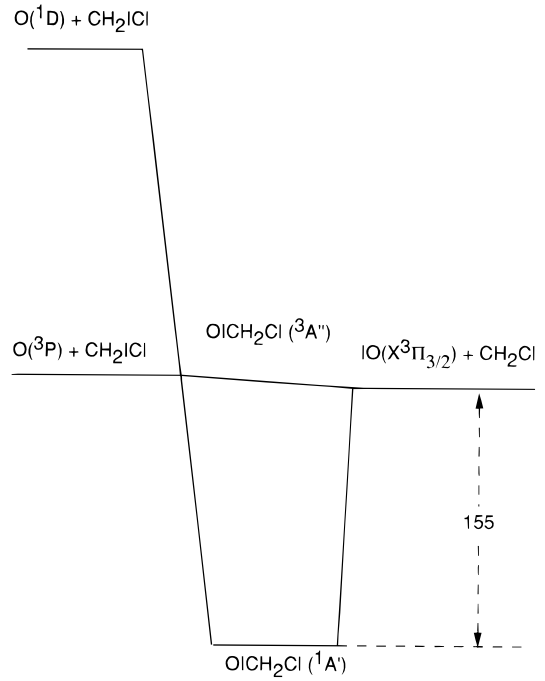

Figure 7. Potential energy profiles for the O + CH_2ICl reaction in bent $OICH_2Cl$ configurations, showing the intersection of the lowest singlet and triplet potential energy surfaces. Symbols refer to electronic symmetry about the OIC bonds.

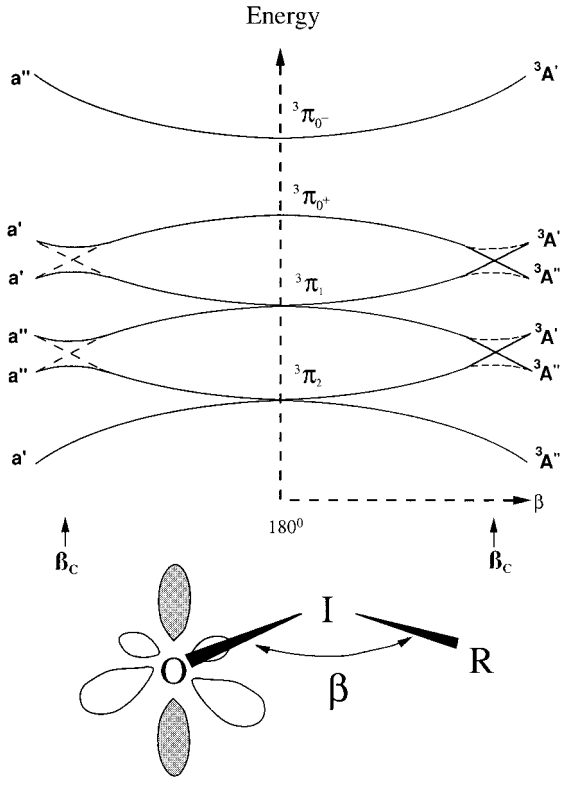

Figure 8. Schematic correlation diagram for triplet states with Renner Teller and spin−orbit interaction in slightly bent $OICH_2Cl$ configurations with OIC interbond angle β. Diabatic Renner Teller curves are shown crossing ^{3}A′ and ^{3}A″ states at the crossing angle β_c. Adiabatic spin−orbit multiplet states show avoided crossings of a′ and a″ states. Symbols refer to electronic symmetry about the OIC bonds.

lowering of the ^{3}A″ Renner Teller surface is enhanced by charge-transfer interaction of the form OI^+R^-. The substantial electron affinity[21] of the CF_3 radical A(CF_3) ∼ 172 kJ mol^{-1} promotes such charge transfer and lowering of the ^{3}A″ potential

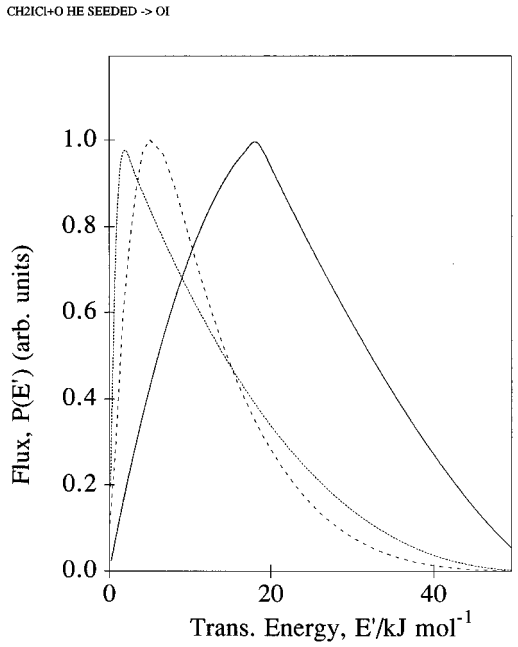

Figure 9. Product translational energy distribution for IO scattering at E of ~46 kJ mol^{-1} from phase space theory (dashed curve) compared with slow (dotted curve) and fast (solid curve) components of the experimental distribution.

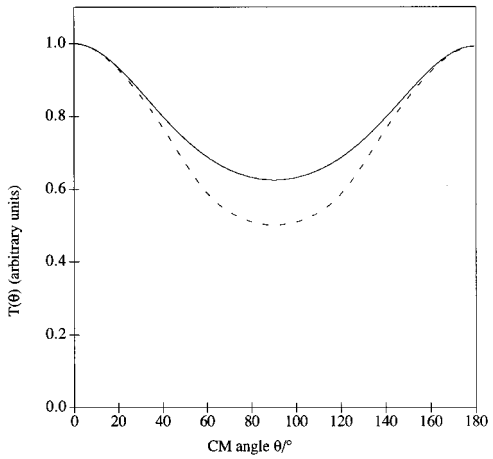

Figure 10. Angular distribution of IO scattering at E of ~46 kJ mol^{-1} calculated from the extended phase space theory (broken curve) compared with the experimental distribution (solid curve).

TABLE 3: Parameters for Extended-Phase Space Theory: Maximum Initial b_m and Final b'_m Impact Parameters, Fitting Parameters c_0, c_2, c_4, and a_2, and Reactant Angular Momentum Parameter cos γ

b_m, Å	b'_m, Å	c_0	c_2	c_4	a^2	cos γ
2.5	5.0	0.02	0.16	0.60	1.84	0.3

energy surface in strongly bent configurations yields strong sideways scattering, whereas restriction of the crossing angle β_c close to $\beta = 180°$ inhibits the contribution of sharply backward peaked scattering. Although the CH_2Cl^- anion has recently been observed[22] in a flowing afterglow experiment, the electron affinity of the CH_2Cl radical is thought to be much lower than that of the CF_3 radical. Hence, charge transfer interaction is expected to play a weaker role in lowering the $^3A''$ potential energy surface, thus allowing the crossing angle β_c to move to smaller values for the O + CH_2ICl reaction. This result provides a wider range of nearly collinear configurations with $180° > \beta > \beta_c$, which can contribute to sharply backward peaked scattering for O + CH_2ICl than is the case for O + CF_3I. The relative intensity of sideways scattering arising from direct dynamics over the $^3A''$ potential energy surface in strongly bent configurations with $\beta_c > \beta > 90°$ may also be depleted by intersystem crossing to the singlet $^1A'$ potential energy surface. However the probability of intersystem crossing of ~1/4 estimated for O + CH_2ICl is lower than that ~1/2 previously estimated[4] for O + CF_3I, in accord with a stronger propensity for the collinear OIR configuration for O + CH_2ICl.

The backward peaking shown by the fast component of IO scattering in Figure 5 is sharper than that predicted[23] for hard sphere scattering even when reaction is confined to the collinear configuration. Similarly sharp backward scattering is also exhibited by the O + C_3H_5I reaction at higher initial translational energy E of ~46 kJ mol^{-1}, where this has also been attributed to direct dynamics over the triplet potential energy surface for this more exoergic reaction. The direct hard sphere scattering model of Zhu et al.[23] suggests that sharp backward scattering requires the range of initial impact parameters to be restricted to less than the hard sphere radius by the presence of a potential energy barrier. Figure 8 suggests that reactive trajectories on the $^3A'$ Renner Teller surfaces correlating with the $^3\Pi_2$ and $^3\Pi_1$ spin multiplet states are more constrained to react in near collinear configurations than are trajectories on the corresponding $^3A''$ Renner Teller surfaces, which tend toward more strongly bent configurations. Interchange can occur between these surfaces via the avoided intersections at the crossing angle β_c. When Renner Teller interaction is strong this is likely to divert trajectories from the upper $^3A'$ to the lower $^3A''$ potential energy surface,[24] particularly if motion over the $^3A'$ surface is impeded by a potential energy barrier. Hence, an initial translational energy threshold for the appearance of sharply backward peaked scattering[3] may reflect a potential energy barrier on the higher $^3A'$ rather than the lower $^3A''$ potential energy surface.

Phase space theory[25] predicts the product translational energy distribution arising from the dissociation of a long-lived collision complex when this is unimpeded by any potential energy barrier in the exit valley of the potential energy surface. The prediction calculated with initial $b_m = 2.5$ Å and final $b'_m = 5$ Å maximum impact parameters and using the vibrational frequencies of CH_2Cl from Jacox[26] and that of IO from Huber and Herzberg[27] is shown in Figure 9 for an initial translational energy E of ~46 kJ mol^{-1}. This result is in good agreement with the product translational energy distribution for the slow component but lies well below that for the fast component. The angular distribution may be calculated by the extended phase space model[28] as a linear combination of angular functions:

$$I(\theta) = c_0 + \frac{1}{2}c_2 I(s = 3/2, a^2 = 1, \cos\gamma, \theta) + \frac{3}{8}c_4 I(s = 5/2, a^2, \cos\gamma, \theta) \quad (4)$$

The coefficients c_0, c_2, and c_4 and the parameter a^2 listed in Table 3 are determined from the phase space calculation and the parameter cos $\gamma = J_{mp}/L_m$, representing the effect of CH_2ICl rotational angular momentum is the ratio of the most probable value $J_{mp} \sim 40\hbar$ to the maximum initial orbital angular momentum $L_m \sim 140\hbar$. The phase space prediction gives a good fit to the experimental angular distribution in Figure 10. This symmetrical angular distribution[29] corresponds to a lifetime of the collision complex of many rotational periods, thus confirming that the slow component of IO scattering in Figure 5 arises

from a long-lived singlet $OICH_2Cl$ complex. The ratio of the lifetime τ to the rotational period τ_{rot} may be estimated for the singlet $OICH_2Cl$ complex with a well depth E_0 of ~155 kJ mol^{-1} from the RRKM formula[30]:

$$\frac{\tau}{\tau_{rot}} \cong \frac{L_m}{2\pi I_2^* \nu}\left\{\frac{E + \Delta D_0 + E_0}{E + \Delta D_0}\right\}^{s-1} \quad (5)$$

This yields $\tau \sim 8\tau_{rot}$ for $E = 46$ kJ mol^{-1} when using a maximum initial orbital angular momentum L_m of ~140 $\hbar$, a moment of inertia $I_2^* \sim 1.2 \times 10^{-44}$ kg m^2, a geometric mean vibrational frequency $\nu = 1.1 \times 10^{13}$ s^{-1}, and an effective number of modes $s = 6$ corresponding to the heavy atom motion with frequencies estimated from ab initio calculations[17] for $OICH_3$ and spectroscopic values[26] for CH_2Cl. This situation assumes an equal probability of dissociation to products and back to reactants.

Acknowledgment. Support of this work by the Engineering and Physical Sciences Research Council and the European Commission is gratefully acknowledged as is the hospitality of the Centre for Interdisciplinary Research of the University of Bielefeld where the manuscript was written.

References and Notes

(1) Wang, J. J.; Smith, D. J.; Grice, R. J. Phys. Chem., **1996**, *100*, 6620.
(2) Wang, J. J.; Smith, D. J.; Grice, R. *J. Phys. Chem.* **1996**, *100*, 13603.
(3) Wang, J. J.; Smith, D. J.; Grice, R. *J. Phys. Chem. A* **1997**, *101*, 3293.
(4) Wells, D. D.; Mohr, S., Goonan, K. M.; Hammer, M.; Grice, R. *J. Phys. Chem. A* **1997**, *101*, 7499.
(5) Gao, X.; Essex-Lopresti, J.; Munro, S., Hall, M. P.; Smith, D. J.; Grice, R. *J. Chem. Soc., Faraday Trans.* **1997**, *93*, 4119.
(6) Klaassen, J. J.; Lindner, J.; Leone, S. R. *J. Chem. Phys.* **1996**, *104*, 7403.
(7) Loomis, R. A.; Klaassen, J. J.; Lindner, J.; Christopher, P. G.; Leone, S. R. *J. Chem. Phys.* **1997**, *106*, 3934.
(8) Rattigan, O. V.; Shallcross, D. E.; Cox, R. A. *J. Chem. Soc., Faraday Trans.* **1997**, *93*, 2839.
(9) Gorry, P. A.; Grice, R. *J. Phys. E* **1979**, *12*, 857.
(10) Nowikow, C. V.; Grice, R. *J. Phys. E* **1979**, *12*, 515.
(11) Entemann, E. A.; Herschbach, D. R. *Discuss. Faraday Soc.* **1967**, *44*, 289.
(12) Radlein, D. St. A. G.; Whitehead, J. C.; Grice, R. *Nature (London)* **1975**, *253*, 37.
(13) Buss, R. J.; Sibener, S. J.; Lee, Y. T. *J. Phys. Chem.* **1983**, *87*, 4840.
(14) Seetula, J. A. *J. Chem. Soc., Faraday Trans.* **1996**, *92*, 3069.
(15) Holmes, J. L.; Lossing, F. P. *J. Am. Chem. Soc.* **1988**, *110*, 7343.
(16) Bedjanian, Y.; LeBras, G.; Poulet, G. *J. Phys. Chem. A* **1997**, *101*, 4088.
(17) Misra. A.; Berry, R. J.; Marshal, P. *J. Phys. Chem. A* **1997**, *101*, 7420.
(18) Stevens, J. E.; Qiang, C.; Morokuma, K., private communication.
(19) Clark, R. J. H.; Dann, J. R. *J. Phys. Chem. A* **1997**, *101*, 2074.
(20) Herzberg, G. *Electronic Spectra of Polyatomic Molecules*; Van Nostrand Reinhold: New York, 1966.
(21) Miller, D. M.; Allen, W. D.; Schaefer, H. F. *Mol. Phys.* **1996**, *88*, 727.
(22) O'Hair, R. A. J.; Gronert, S.; DePuy, C. *Eur. Mass. Spectrom.* **1995**, *1*, 429.
(23) Zhu, Z. Z.; McDouall, J. J. W.; Smith, D. J.; Grice, R. *Chem. Phys. Lett.* **1992**, *188*, 520.
(24) White, R. W. P.; Smith, D. J.; Grice, R. *Chem. Phys. Lett.* **1992**, *193*, 269.
(25) Light, J. C. *Discuss. Faraday Soc.* **1967**, *44*, 14.
(26) Jacox, M. E. *J. Phys. Chem. Ref. Data* 1990, 19, 1387.
(27) Huber, K. P.; Herzberg, G. *Constants for Diatomic Molecules*; Van Nostrand Reinhold: New York, 1979.
(28) Wang, J. J.; Smith, D. J.; Grice, R. *Chem. Phys.* **1996**, *207*, 203.
(29) Fisk, G. A.; McDonald, J. D.; Herschbach, D. R. *Discuss. Faraday Soc.* **1967**, *44*, 228.
(30) White, R. W. P.; Smith, D. J.; Grice, R. *J. Phys. Chem.* **1993**, *97*, 2123.